Experimental and Analytical Study of Close-Coupled Ventral Nozzles for ASTOVL Aircraft

Jack G. McArdle and C. Frederic Smith
Lewis Research Center
Cleveland, Ohio

NASA

EXPERIMENTAL AND ANALYTICAL STUDY OF CLOSE-COUPLED
VENTRAL NOZZLES FOR ASTOVL AIRCRAFT

Jack G. McArdle
National Aeronautics and Space Administration
Lewis Research Center
Cleveland, Ohio, U.S.A

and

C. Frederic Smith
Sverdrup Technology, Inc.
Cleveland, Ohio, U.S.A

Abstract

Flow in a generic ventral nozzle system
was studied experimentally and analyti-
cally with a block version of the
PARC3D computational fluid dynamics
program (a full Navier-Stokes equation
solver) in order to evaluate the pro-
gram's ability to predict system per-
formance and internal flow patterns.
For the experimental work a one-third-
size model tailpipe with a single large
rectangular ventral nozzle mounted
normal to the tailpipe axis was tested
with unheated air at steady-state pres-
sure ratios up to 4.0. The end of the
tailpipe was closed to simulate a
blocked exhaust nozzle. Measurements
showed about 5½-percent flow-turning
loss, reasonable nozzle performance
coefficients, and a significant aftward
axial component of thrust due to flow
turning more than 90°. Flow behavior
into and through the ventral duct is
discussed and illustrated with paint
streak flow visualization photographs.
For the analytical work the same ven-
tral system configuration was modeled
with two computational grids to evalu-
ate the effect of grid density. Both
grids gave good results. The finer-
grid solution produced more-detailed
flow patterns and predicted performance
parameters, such as thrust and dis-
charge coefficient, within 1 percent of
the measured values. PARC3D flow visu-
alization images are shown for compari-
son with the paint streak photographs.
Modeling and computational issues
encountered in the analytical work are
discussed.

Introduction

Improved short takeoff and vertical
landing (STOVL) aircraft are planned
for possible future development. For
these aircraft the same propulsion sys-
tem will provide power for lift and
hover as well as for supersonic hori-
zontal flight. The propulsion system
must have high-thrust-to-weight-ratio
engines; efficient gas ducting and
thrusters; large, reliable valves and
seals; and integrated engine and flight
controls. To develop the required
technology for these aircraft, the NASA
Lewis Research Center has established
active programs in mission analysis,
integrated controls, lift thrusters,
and hot gas reingestion in hover
flight.

When the STOVL propulsion system is
operating in the lift mode, the rear
jet nozzle will be blocked, and valves
will be opened to duct engine exhaust
gases to two or more thrusters directed
downward. In many proposed configura-
tions one of the lift thrusters will be
a ventral nozzle. A typical arrange-
ment is sketched in Fig 1. The ventral
nozzle draws mixed core and fan gases
from the engine tailpipe through a
valve and opening having no inlet turn-
ing vanes. The ventral nozzle size and
location are chosen to balance the
pitching moment from thrusters forward
of the aircraft center of gravity dur-
ing hover flight. Close coupling is
necessary because the valve and the
nozzle must be wholly mounted within
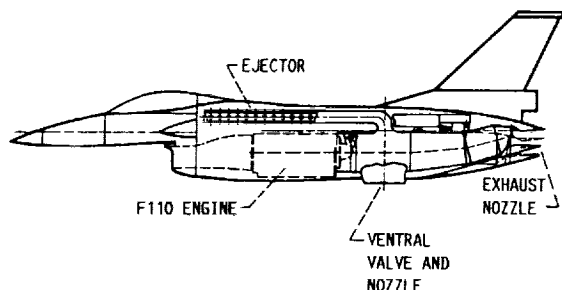the fuselage. The ventral nozzle also

FIG 1. - PROPOSED STOVL PROPULSION SYSTEM WITH VENTRAL NOZZLE, ON E7D AIRCRAFT MODEL.

may be vectored to provide trim or pitch control.

Early work on STOVL deflectors was reported in Refs 1 and 2 and included experiments examining the internal flow field and performance of model turbofan engine and ventral nozzle configurations. However, no reports of computational fluid dynamics (CFD) analyses of ventral flow were found in the literature. In an ongoing Lewis program ventral nozzle performance is being studied experimentally and analytically. A generic model tailpipe (about one-third of full size) having a single large, rectangular ventral nozzle mounted normal to its axis was built and tested with unheated air. A blind flange at the end of the tailpipe simulated a blocked exhaust nozzle. Analytical performance of the same tailpipe and ventral nozzle configuration was modeled and studied with a CFD code called PARC3D, using Cray computers. PARC3D solves the three-dimensional, compressible-flow Navier-Stokes equations and includes an algebraic turbulence model. A block version of PARC3D was used to simplify construction of the chosen computational grid and to reduce the computer requirements for a fairly complex geometry. Two grids for the same configuration were generated to evaluate the effect of grid density on the numerical results.

The major objectives of the work reported in this paper were to expand understanding of ventral flow turning by appropriate tests, and to evaluate the ability of the chosen computational grids and CFD code to predict the experimental performance. The results are shown in performance plots for

steady-state ratios of tailpipe to ambient pressure up to 4.0, internal paint streak flow visualization photographs, and CFD flow visualization images for direct comparison with the experimental photographs at a pressure ratio of 3.0.

Apparatus and Instrumentation

Test Stand

The model was tested on the Powered Lift Facility (PLF) at the NASA Lewis Research Center. The PLF is a unique outdoor stand designed to measure simultaneous axial (thrust), normal (lift), and side forces up to 25 000 lb (110 kN). The stand was supplied with unheated air from the central system at 150-psi (1000-kPa) pressure. Airflow was controlled by a valve in the facility inlet line. Flow rate was measured with an ASME long-radius nozzle. The model mounted on the PLF stand is shown in Fig 2. The model was mounted with the ventral nozzle discharging upward for operational convenience.

Model

A sketch of the model tailpipe and ventral nozzle is shown in Fig 3. An uncomplicated design was chosen in order to simplify the computational grid generation. The tailpipe was 13.5 in. (34.3 cm) in diameter, which is about one-third the size of many current military engines. The model was connected to the 24-in. (61-cm) diameter facility mounting flange through a conical-plus-cylindrical transition section. This section con-

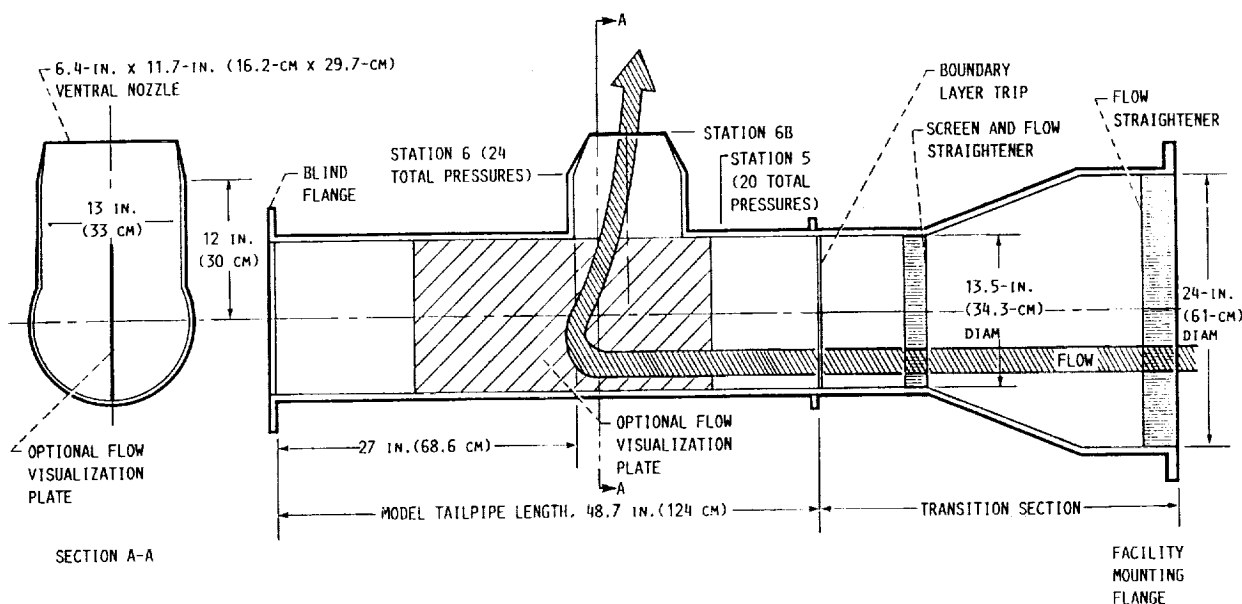FIG 2. - MODEL MOUNTED ON POWERED LIFT FACILITY TEST STAND.

2

FIG 3. - EXPERIMENTAL MODEL OF TAILPIPE/VENTRAL NOZZLE.

tained two honeycomb flow straighteners and one fine-mesh screen, just ahead of the model, designed to provide uniform inflow. The screen was 14 mesh by 0.009-in. (0.23-mm) wire, and on the basis of results reported in Ref 3, was relied on to reduce free-stream turbulence intensity to less than 1/2 percent. In addition, a toothed metal strip protruded 0.06 in. (1.5 mm) from the wall to ensure that the inflow boundary layer was turbulent. A blind flange was located two tailpipe diameters downstream of the ventral opening to simulate a blocked exhaust nozzle. The rectangular convergent ventral nozzle was mounted on a duct 0.89 tailpipe diameter long (measured from the tailpipe centerline). The intersecting edges of the ventral duct and tailpipe, at the ventral cutout, were not rounded. These "square" edges were intended to represent a worst-case design condition.

An optional flow visualization plate, 0.06 in. (1.5 mm) thick, could be mounted on the vertical centerline (a plane of symmetry) of the model over the ventral opening. The plate extended one tailpipe diameter downstream of the opening to capture flow patterns in the tailpipe. The plate was not installed for performance tests or flow visualization photographs of the tailpipe and ventral duct walls.

Instrumentation

The model instrumentation stations are shown in Fig 3. Tailpipe pressure (P5) was measured with five total-pressure tubes on each of four equally spaced rakes at station 5. Ventral nozzle inlet pressure (P6) was measured with 24 total-pressure tubes (20 tubes arranged uniformly in the duct plus 4 corner tubes) at station 6. The wall pressure at several locations on the model was measured with static-pressure taps. Ventral nozzle exit flow conditions were measured by probes driven across the nozzle just downstream of the exit plane by an electric actuator. For one test a three-tipped total-pressure probe was used to map the pitot-pressure distribution. For another test a calibrated conical probe was used to measure total pressure, as well as flow angles relative to the probe tip, as functions of the measured tip and surface pressures. Airflow, forces, air temperature, and ambient conditions were measured by facility instrumentation systems using calibrated load cells and other conventional transducers.

Procedure

Performance Tests

After force system tares had been

3

obtained, steady-state thrust and air-flow performance was measured at several ratios of tailpipe to ambient pressure (PR5) up to 4.0. The data were recorded on the central laboratory system and batch processed on a mainframe computer.

Exit Surveys

The flow-angle probe and total-pressure rake data were obtained at selected locations in the exit flow (station 6B) at PR5 = 3. The data were processed along with the performance test data.

Flow Visualization

After the optional flow visualization plate had been installed, dabs of thick, oily paint were applied to the plate with a syringe in a grid-like pattern. In order to minimize transient flow effects, airflow was started quickly, held at PR5 = 3 for 1 min, and then quickly shut down. The flow caused the paint to run along streamlines, and the resulting streaks provided a clear picture of the flow pattern. A similar procedure was followed without the plate installed to obtain flow visualization photographs at the ventral duct walls.

Computational Fluid Dynamics

A major objective in these studies was to evaluate the ability of a chosen computational grid and CFD code to predict the internal flow patterns and overall performance of a ventral nozzle system. To this end, the PARC3D code was chosen because it is familiar to NASA Lewis researchers and because it is known to be applicable to flow problems of the same general type. The same tailpipe and ventral nozzle configuration used for the experimental work was modeled as described in the following paragraphs.

PARC3D Code

The PARC3D code was originally developed at the NASA Ames Research Center (Ref 4) to analyze external flows. It solves the three-dimensional, compressible-flow, Navier-Stokes equations in curvilinear coordinates and
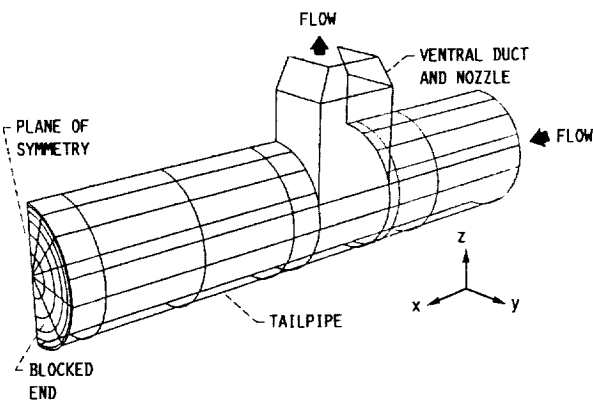
includes the Baldwin-Lomax (algebraic) turbulence model (Ref 5). The code later was modified at the U.S. Air Force Arnold Engineering Development Center (Ref 6) for use with internal flows. The equations of motion are solved by using Beam and Warming's approximate factorization scheme. Pulliam's scalar pentadiagonal transformation is applied to uncouple the equations of motion.

A block version of the PARC3D code was used in this study. The block version allows the computational grid to be broken into two or more blocks to simplify modeling. Trilinear interpolation is used to exchange computational information between modeling blocks (Ref 7). As an additional advantage, most of the information required in the core memory is associated with the current block, thus reducing computer storage needs.
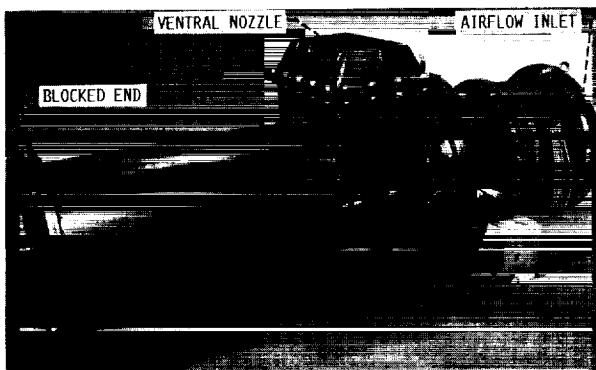
Computational Grid

Because the experimental configuration had a plane of symmetry, only one of the symmetric halves was modeled. The grid model was broken into two blocks. The tailpipe made up one block, which was modeled by using an O-grid. The O-grid consisted of concentric circles parallel to the tailpipe surface and radial lines normal to the surface. The ventral duct and nozzle made up the other block and were modeled by using an H-grid. The H-grid consisted of lines parallel and perpendicular to the walls. This approach provided body-conforming grids for each block. A "wire" diagram of the grid model is shown in Fig 4 along with a photograph of the experimental model for comparison.

Both grids were generated algebraically by the INGRID3D code (Ref 8). The grids were stretched by hyperbolic functions in order to pack grid points near the walls and the center of the O-grid. Two grids of the same model were made to evaluate the effects of grid density on the predicted flow field and numerical results. The first grid, called herein the "coarse" grid and shown in Fig 5, contained 31 875 points in each block (51X25X25 points
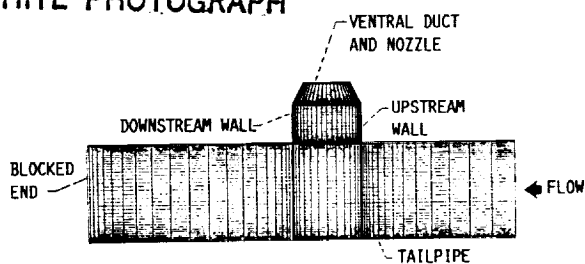
FLOW

VENTRAL DUCT
AND NOZZLE

PLANE OF
SYMMETRY

FLOW

z

x   y

TAILPIPE

BLOCKED
END

(a) ANALYTICAL "WIRE" DIAGRAM. ONLY ONE-HALF IS USED FOR CFD;
FOR CLARITY MANY OF THE GRID LINES ARE NOT SHOWN.

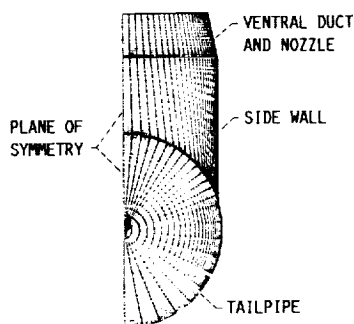VENTRAL NOZZLE   AIRFLOW INLET

BLOCKED END

(b) EXPERIMENTAL MODEL.

FIG 4. - VENTRAL SYSTEM CONFIGURATION.

VENTRAL DUCT
AND NOZZLE

DOWNSTREAM WALL   UPSTREAM
WALL

BLOCKED
END   FLOW

TAILPIPE

(a) PLANE OF SYMMETRY (xz-PLANE).

VENTRAL DUCT
AND NOZZLE

PLANE OF   SIDE WALL
SYMMETRY

TAILPIPE

(b) END VIEW (yz-PLANE).

FIG 5. - "COARSE" COMPUTATIONAL GRID.

VENTRAL DUCT
AND NOZZLE

DOWNSTREAM WALL   UPSTREAM WALL

BLOCKED
END   FLOW

TAILPIPE

(a) PLANE OF SYMMETRY (xz-PLANE).

VENTRAL DUCT
AND NOZZLE

SIDE WALL

PLANE OF
SYMMETRY

TAILPIPE

(b) END VIEW (yz-PLANE).

FIG 6. - "FINE" COMPUTATIONAL GRID.

in the streamwise and other coordinate
directions, respectively). This grid
size was limited by the space available
on the Cray X-MP computer at Lewis but
was suitable to demonstrate the appli-
cability of the PARC3D code to this
problem. So that an adequate number of
points could be provided in the central
region of the ventral nozzle, packing
near the nozzle walls was limited and
the closest grid point was 0.1 in.
(2.5 mm) from the surface. Good ana-
lytical results were obtained with this
grid.

The second grid, called herein the
"fine" grid and shown in Fig 6, con-
tained 262 701 (101X51X51) points in
each block. In the ventral duct and
nozzle block the grid was packed so
that the closest point was 0.01 in.
(0.25 mm) from the nozzle surface. In
the tailpipe the closest point was
0.01 in. (0.25 mm) from the wall sur-
face, the same as in the coarse grid.
Comparison of Figs 5 and 6 illustrates
the denser grid packing near the model
walls and near the tailpipe centerline
obtained with the fine grid. Packing
near the centerline minimized the
effects of the "pole" boundary condi-
tion, which is discussed in the next
section.

5

Boundary Conditions

The boundary conditions for this problem are shown in Fig 7. Analysis of the jet plume outside the nozzle was not performed because it would unduly enlarge the computational grid. However, proper modeling of the flow at the nozzle exit is very important. The nozzle has a convergent shape, and the transonic flow at the exit complicates the boundary conditions. This problem was resolved by adding a fictitious divergent section of suitable size to the ventral nozzle to provide supersonic flow at the exit of the computational domain. Flow properties could then be extrapolated downstream of the area of interest, and the nozzle throat was modeled as if the external plume were included. Previous work has shown that this is a good approach to modeling a three-dimensional convergent nozzle.

A problem also occurs at the center of the tailpipe O-grid, where the radial grid lines become coincident. This would cause singularity problems in calculating the coordinate transfor-

mation derivatives (metrics). This problem was circumvented by using a "pole" boundary condition at the center of the O-grid. In this case the flow properties were averaged around the adjacent grid line, and these values were applied to all points along the innermost grid line, which had a radius of about 1 percent of the tailpipe radius.

Results and Discussion

This portion of the paper first reports the results of the performance testing at steady-state ratios of tailpipe to ambient pressure (PR5) up to 4.0 and shows the results of the PARC3D computations at PR5 = 2.96. Next, the internal flow patterns are described by using the paint streak photographs and CFD particle trajectory plots. The particle trajectory plots were produced by the PLOT3D code (Ref 9) from the PARC3D numerical results. Finally, modeling and computational issues encountered in the analytical work are discussed.

The pressure ratio PR5 was chosen for presentation of the results because the tailpipe pressure is most important to engine operation and must be held constant during ventral system use to keep the engine running at the same operating point.

Ventral System Performance

The gas stream lost energy in turning from the tailpipe into the ventral duct, resulting in decreased average total pressure. For STOVL aircraft the flow-turning loss can limit the maximum available ventral thrust during hover flight. The loss measured in the model tested, shown in Fig 8, was about 5½ percent when the tailpipe pressure ratio was greater than 2. The loss computed by the PARC3D program at PR5 = 2.96 was only slightly higher. This magnitude should be typical of ventral system designs of this general type and size. Turning vanes or a rounded shape at the ventral inlet could reduce the loss but might be difficult to package in the small available fuselage space along with a shutoff valve and other hardware needed

EXTRAPOLATE
(MACH NUMBER >1)

—FICTITIOUS DIVERGENT SECTION

—TRUE NOZZLE EXIT PLANE

—NO SLIP, ADIABATIC

—INTERPOLATE

POLE —

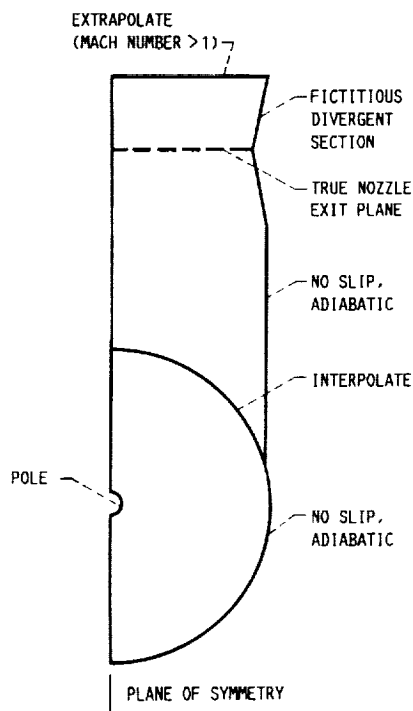—NO SLIP, ADIABATIC

PLANE OF SYMMETRY

FIG 7. - BOUNDARY CONDITIONS. TOTAL PRESSURE AND TOTAL TEMPERATURE WERE SPECIFIED FOR UP-STREAM PORTION OF TAILPIPE; ADIABATIC CONDITIONS AND NO SLIP WERE SPECIFIED FOR DOWNSTREAM PORTION OF TAILPIPE.
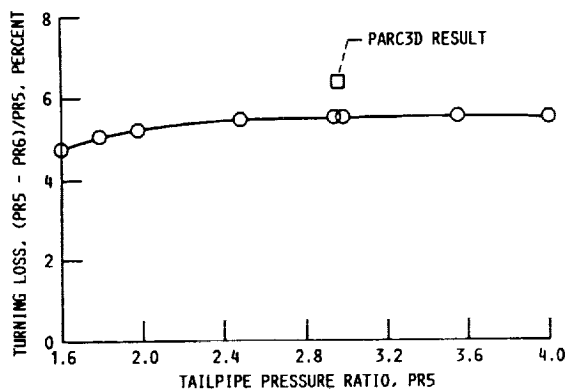
FIG 8. - TOTAL-PRESSURE FLOW-TURNING LOSS.

at the tailpipe opening. The data in Fig 8 show that the loss was less at lower tailpipe pressure ratios. This trend implies that flow-turning loss is dependent on tailpipe velocity or Mach number; therefore, the loss should be lower in other similar configurations with smaller ventral nozzles. Both the measured and analytical system performance are given in Fig 9 and Table I[i]. For the ventral system tested, the discharge and thrust coefficients based on tailpipe conditions, shown by the open symbols in Figs 9(a) and (b), were lower than typical for a simple conical nozzle. However, this effect is due to the flow-turning loss. The coefficients rose to more normal levels when computed in the conventional manner, by using the averaged nozzle inlet total-pressure ratio (PR6) as shown by the solid symbols. The PARC3D results and the experimental data are in excellent agreement. Both

[i] For these results the parameters are defined as follows: (1) discharge coefficient, the measured flow rate divided by the ideal flow rate at the same inlet conditions and pressure ratio; (2) total thrust coefficient, the measured total thrust divided by the ideal thrust produced by the measured flow at the same inlet conditions and pressure ratio; (3) referred flow rate, the measured flow rate times $\sqrt{\theta}$ divided by δ, where θ is the flow total temperature divided by 518.7 °R and δ is the flow total pressure divided by 14.696 psi; (4) referred thrust, the measured thrust divided by δ.

the measured and CFD-predicted forces show a negative thrust component, although the ventral nozzle axis was normal to the tailpipe centerline. This negative force is interpreted to mean that the jet had effectively turned more than 90°, as plotted in Fig 9(c). The axial force measured 7 to 10 percent of the ventral nozzle total thrust (Fig 9(d)); the PARC3D-computed force also was about 7 percent. In a STOVL aircraft the axial force would tend to accelerate the craft backward but could be overcome by vectoring the ventral nozzle or opening some other thruster to produce a counteracting force.

The measured and predicted ventral system performances are compared in more detail in Table I. Both the coarse- and fine-grid results are in very good agreement with the measured values. In some cases the fine-grid values are slightly closer to the experimental data, but the coarse-grid computations
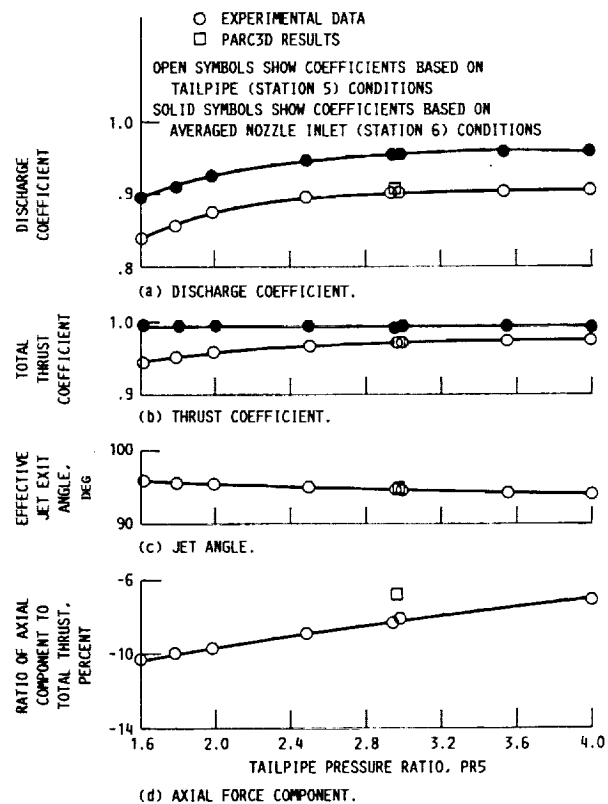

FIG 9. - VENTRAL SYSTEM PERFORMANCE.

TABLE I. - VENTRAL SYSTEM PERFORMANCE

	CFD results		Experimental
	Coarse grid	Fine grid	
Ratio of tailpipe to ambient pressure, PR5	2.97	2.96	2.96
Ratio of nozzle inlet to tailpipe pressure, PR6	0.932	0.935	0.945
Nozzle discharge coefficient based on P5	0.88	0.91	0.91
Nozzle thrust coefficient based on P5	0.96	0.97	0.97
Nozzle flow rate referred to P5, lb/sec	22.67±0.2	23.32±0.04	23.04±0.12
Nozzle total thrust referred to P5, lb	870±9	905±2	896±10
Nozzle axial thrust referred to P5, lb	-88	-72	-73

may be quite acceptable for screening candidate configurations or otherwise estimating expected performance.

Flow Behavior

In this discussion the ventral system is assumed to be installed in an aircraft as illustrated in Fig 1. The results presented here are for a steady-state tailpipe pressure ratio, PR5 = 3. The Mach number at station 5 measured 0.33 on the ventral side of the tailpipe and 0.27 on the opposite side.

Flow in ventral duct - In order to understand the manner in which flow turned from the tailpipe into the ventral opening, a test was made with the optional flow visualization plate installed as illustrated in Fig 3. The paint streaks resulting from this test, along with particle trajectories [ii] computed with the PARC3D code on the model plane of symmetry, are shown in Fig 10. The paint streaks on the plate

(a) COARSE GRID.   (b) FINE GRID.

(c) EXPERIMENT.

(d) PREDICTION.

FIG 10. - TAILPIPE PLANE-OF-SYMMETRY FLOW VISUALIZATION.

[ii] A particle trajectory is the path a massless particle would take as it flowed through the ventral system.

8

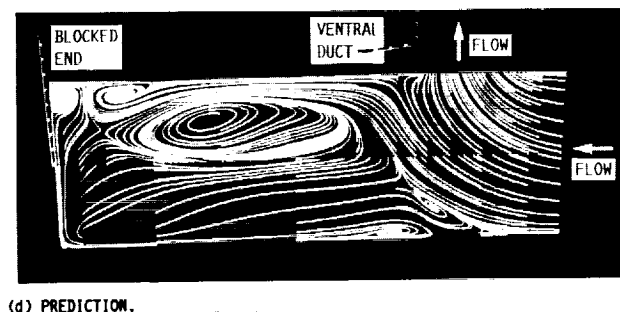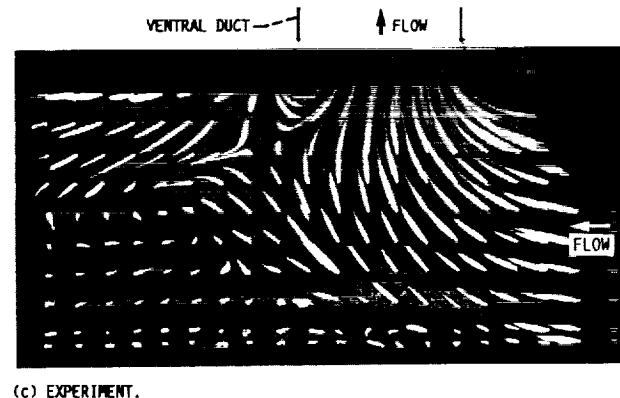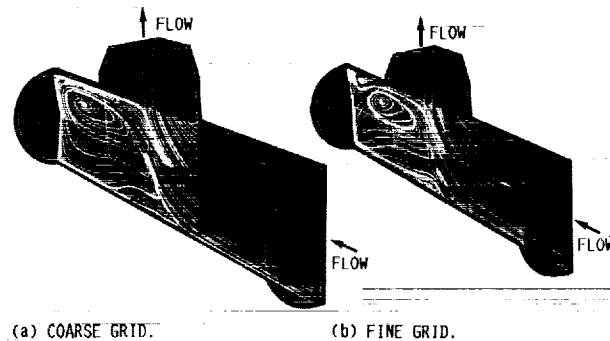show that the flow did not turn sharply but rather split so that some of the flow made a smooth turn into the opening and some impacted the tailpipe wall to form a stagnation point slightly downstream of the opening. The impacting flow then split, with some flowing back into the ventral opening and some flowing farther into the tailpipe. In the tailpipe it circulated in a counterclockwise direction and returned upstream along the wall opposite the ventral opening.

The PARC3D results give the same general flow patterns. (The discontinuities in the particle paths at the tailpipe centerline, Fig 10(d), resulted because the PLOT3D program did not recognize the pole at the center of the O-grid; however, the PARC3D solution is continuous across the centerline.) The predictions for the fine-grid solution reveal several smaller vortices that are not present in the coarse-grid solution. The predicted center of the larger vortex is farther from the tailpipe centerline than shown by the paint streaks. The reason for this difference may be that the flow visualization plate is a no-slip flow surface, whereas the trajectories were computed along an inviscid plane of symmetry. The recirculating flow was moving along almost all the tailpipe surface at fairly low velocity. The wall flow could affect the cooling-air requirements for ventral systems in STOVL aircraft.

PARC3D velocity vectors (not shown herein) indicate that in the ventral duct the flow was separated from the upstream wall. The separated region was confirmed by measured wall pressures, which were lowest on the upstream wall. The flow continued to turn as it moved through the duct. Continued turning suggests that the flow condition at the ventral nozzle inlet could be influenced by the length and shape of the duct and, in turn, could affect the total performance of the ventral system.

Although the duct flow patterns have been described in two-dimensional terms, in fact the flow was highly three dimensional and many secondary and vortex-like flows existed, as discussed in the next section.

Flow along ventral duct walls - For another flow visualization test the optional plate on the tailpipe centerline was removed, and dabs of paint were applied to the ventral duct and nozzle walls. The next several figures show paint streak photographs from this test and corresponding particle trajectories. Although trajectories were computed only for one of the symmetric halves, in the following discussion a mirror image of each trajectory is assumed to exist in the other half. The mirror image is included in the figures to assist in comparing the experimental and analytical results. The paint streaks and particle trajectories obtained on the front (upstream) ventral wall are shown in Fig 11. Both show that the separated region consisted of twin counterrotating vortices
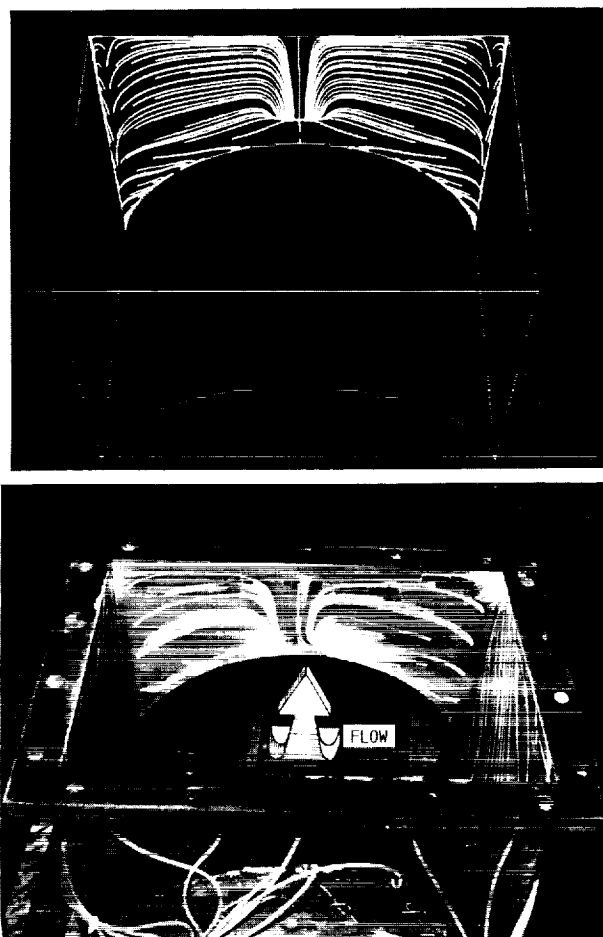

FIG 11. - FLOW VISUALIZATION ON VENTRAL DUCT FRONT WALL.

that drew flow from the outer corners and returned it to the tailpipe near the centerline. Static pressures measured on the front wall were low, indicating high-velocity flow.

Both the paint streaks and the particle trajectories on the side walls (Fig 12) show that the air flowed out of the ventral duct and toward the vortices at the front wall. In the front corners the air turned along the wall toward the nozzle.

Two distinct flow fields can be seen on the rear (downstream) ventral duct wall (Fig 13). Air that entered the duct opening from the downstream part of the tailpipe (Fig 10) set up a recirculation region near the tailpipe cutout revealed by the paint streaks aimed back to the cutout. This flow may have been weak because the paint collected on the sharp edge of the cutout. The recirculation was also seen in the velocity vector field computed by the PARC3D program (not shown here) and in
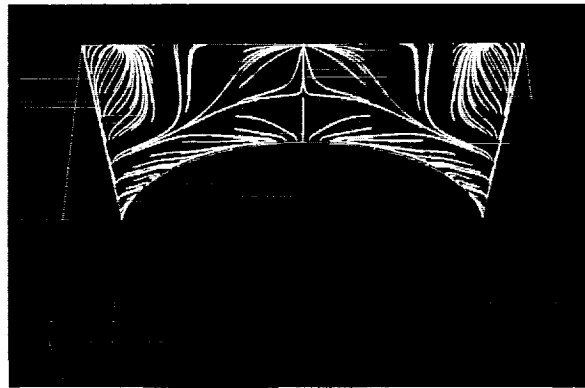

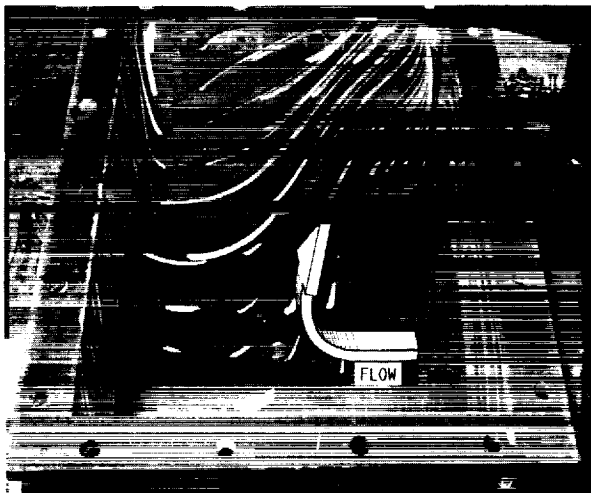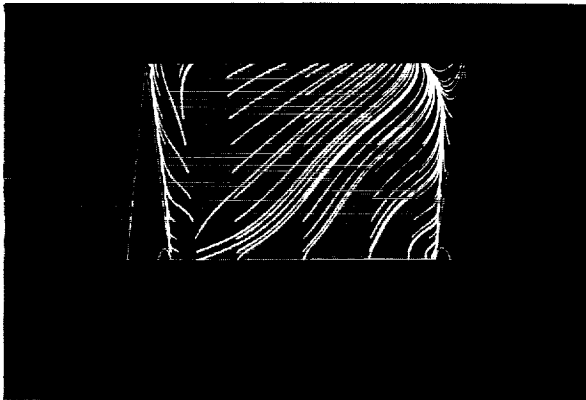FIG 13. - FLOW VISUALIZATION ON VENTRAL DUCT REAR WALL.

the particle trajectories. The main flow, however, went directly along the wall toward the ventral nozzle.

Wall pressure - Experimental and PARC3D static pressures on the tailpipe wall are shown in Fig 14. The measured data clearly show the lower wall pressures caused by flow entering the ventral duct. The pressures predicted by the PARC3D code generally are about 2 percent greater than the measured pressures. The code appears to be less accurate near the downstream edge of the tailpipe opening, where the flow direction suddenly changed at the stagnation region on the tailpipe wall (see Fig 10).

Nozzle exit flow - A flow-angle survey was made in the nozzle exit flow with a conical probe that had direction-sensing pressure ports. Although this survey was made at PR5 = 1.69 (free-stream Mach number, 0.9) because the probe was not calibrated for supersonic flow, the results are considered representative of the exit flow at higher pressure ratios. Two survey traverses

FIG 12. - FLOW VISUALIZATION ON VENTRAL DUCT SIDE WALL.

10

(a) TAILPIPE WALL ON VENTRAL SIDE.

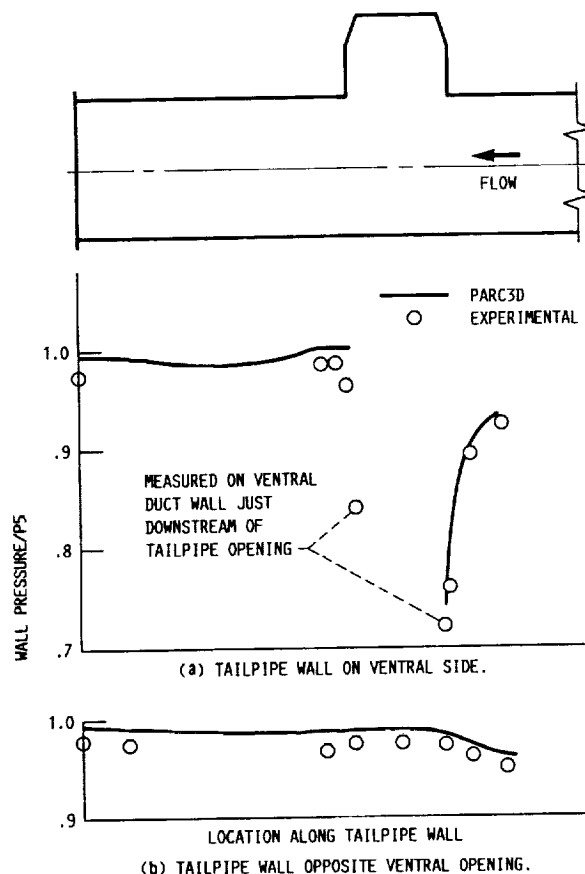(b) TAILPIPE WALL OPPOSITE VENTRAL OPENING.

FIG 14. - TAILPIPE WALL STATIC PRESSURE.

at the exit plane were made: one near an outboard edge of the nozzle (Fig 15(a)), and the other near the plane of symmetry (Fig 15(b)). Near the outboard edge there was little or no pressure loss except near the nozzle forward lip. The flow direction was outboard and forward in the aft part of the nozzle and inboard and forward in the front part. Near the plane of symmetry the measured total pressure was as much as 15 percent less than the average station 5 pressure. The flow directions were similar to the directions nearer the outboard edge, but the flow angles were greater.

The results show that the flow leaving the nozzle was still trying to "fill in" the lower-density region at the center of the upstream wall. Although not measured, mirror images of these patterns must exist on the other side of the plane of symmetry. On that basis the lateral velocity components would cancel but cause a net thrust loss, whereas the axial components would add to cause a net thrust in the

reverse (downstream) direction. These data, then, corroborate and explain the axial force measured by the facility load cells, previously shown in Fig 9.
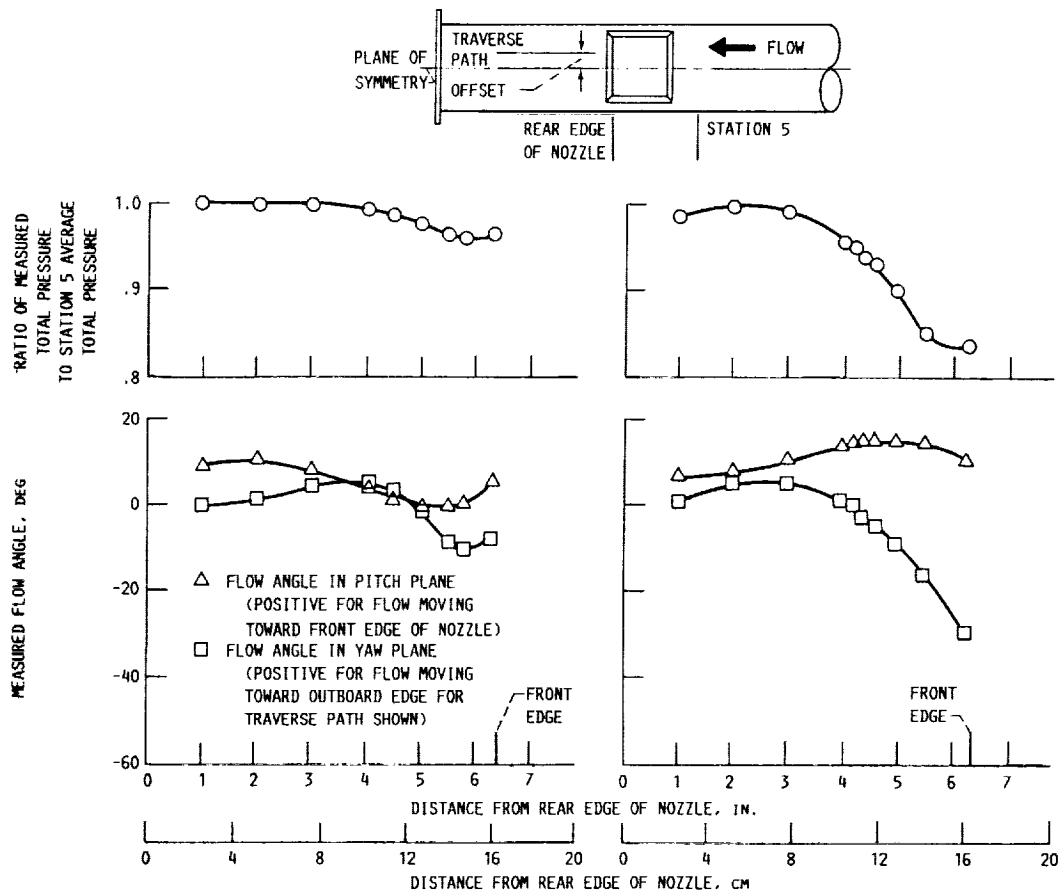
An additional survey of the nozzle exit flow was made with a total-pressure rake. The data from this survey were processed into a pressure contour map at the exit plane, which is shown in Fig 16 together with a similar map computed by the PARC3D code. Only one of the symmetric halves is shown. Results are given for PR5 = 3. The analytical map always shows true total pressure, but the experimental data are pitot pressures, which are less than true total pressure by the normal shock loss at the tip in supersonic flow and by measurement errors when the flow angle relative to the tip is greater than about 15°. Nevertheless, the maps are in good qualitative agreement: both show strong flow in the rear part of the nozzle and an oval-shaped region of weaker flow in the front part.

CFD Modeling and Numerical Issues

Turbulence model - The Baldwin-Lomax algebraic turbulence model was developed for two-dimensional, separated flows. Extension of this model to three-dimensional flows is difficult, especially for cases having multiple walls such as the rectangular ventral duct. For the present problem the turbulent viscosities calculated for each wall were weighted and averaged according to the distance from the point of calculation to the relevant wall. No adjustments to this approach were made along walls in vortical regions. Inaccuracies involved in applying the Baldwin-Lomax model in this manner may have caused part of the differences between the measured and predicted wall static pressures.
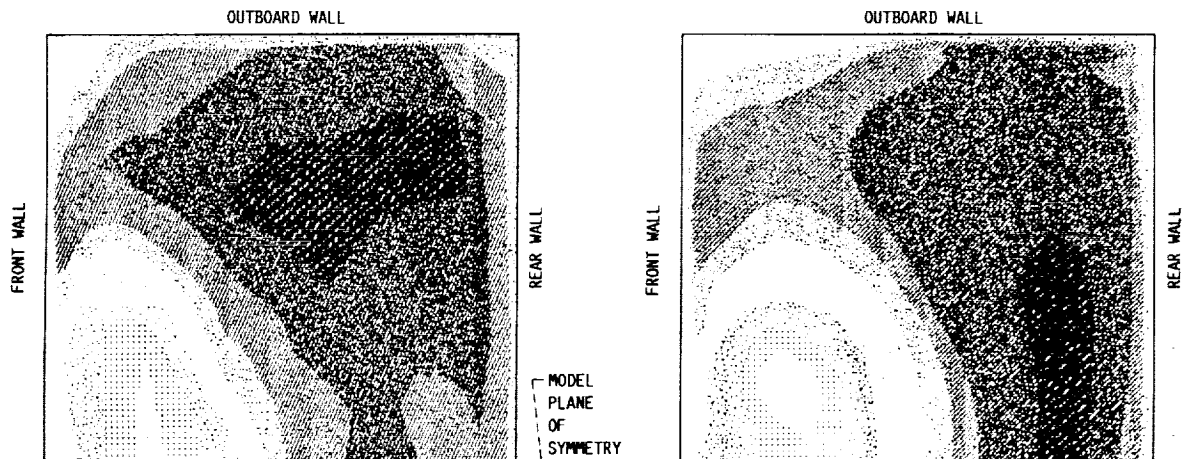
A two-equation turbulence model, such as the k-ε model (Ref 10), would handle multiple walls in a more satisfactory manner but would increase the computation time significantly.

Boundary-layer resolution in ventral duct - Resolution of boundary-layer flow influenced CFD calculations

(a) TRAVERSE PATH OFFSET 4.5 IN. (11.4 CM) FROM PLANE OF SYMMETRY.

(b) TRAVERSE PATH OFFSET 1.5 IN. (3.8 CM) FROM PLANE OF SYMMETRY.

FIG 15. - VENTRAL NOZZLE EXIT FLOW CONDITIONS. RATIO OF TAILPIPE TO AMBIENT PRESSURE, PR5, 1.69.

(a) EXPERIMENTAL PITOT PRESSURE.

(b) ANALYTICAL TOTAL PRESSURE.

FIG 16. - NOZZLE EXIT PLANE PRESSURE CONTOURS. LIGHT SHADINGS INDICATE LOWER PRESSURES. DARK SHADINGS INDICATE HIGHER PRESSURES.

12

related to wall static pressure. For the computational grids used in this problem the y+ distance [iii] for the first grid point of the ventral duct wall was typically 15 for the fine grid. This distance located the point slightly outside the viscous sublayer region of the boundary layer. In order to fully define the boundary layer, the first grid point should be at a y+ distance less than 10 from the wall surface (Ref 11). However, decreasing the first grid point y+ from 150 (for the coarse grid) to 15 (for the fine grid) did not change the calculated wall static pressures significantly. A possible reason for this result is that the ventral duct flow separated at the sharp corners of the tailpipe opening and was still turning in the duct. Thus, because the boundary layer did not build up in the usual way from viscosity and adverse pressure gradients, the referenced y+ criterion may not be applicable.

Conservation of mass - The inlet (station 5) and exit (station 6B) mass flow rates computed by PARC3D with the fine grid are shown in Fig 17 as a function of the cumulative number of iterations. As the solution progressed, the difference between the computed inlet and exit flows diminished. One reason for the flow difference is that the transfer of flow properties at the grid block interface was not forced to be conservative or characteristically correct. When flow convergence was achieved, the residuals (differences in flow properties between successive iterations) had been reduced approximately three orders of magnitude. Further reduction seems to be limited by the turbulence model used or possibly by flow-field unsteadiness in the vortices.

Low Mach number effects - The Mach number in the blocked tailpipe was low, typically 0.1 or less. As with other compressible-flow codes the PARC3D code encountered numerical problems in this
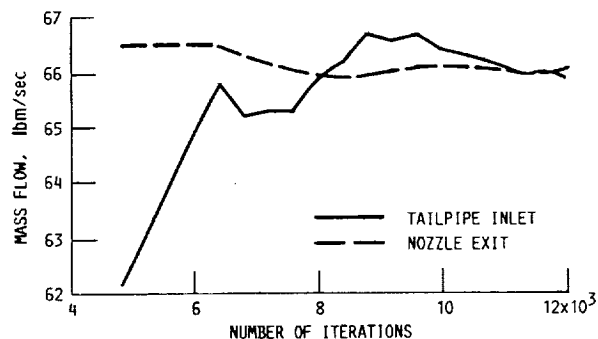

FIG 17. - CALCULATED MASS FLOW RATES AS FUNCTION OF CUMULATIVE NUMBER OF ITERATIONS.

region that led to convergence difficulties. Use of preconditioning (Ref 12) could alleviate this problem.

Computational speed - The maximum Courant-Friedrichs-Lewy (CFL) number (Ref 13) that could be used for both blocks to obtain a stable solution was 1.0 for the coarse grid and 0.5 for the fine grid. (The CFL number limits the iteration step size.) The computational speed for the coarse grid was 800 iterations per CPU hour on the Cray X-MP. The fine-grid speed was 200 iterations per CPU hour on the Cray Y-MP. The coarse-grid solution required approximately 4000 iterations; the fine-grid solution required 12 000 iterations.

Concluding Remarks

Experimental and analytical flow studies of the same generic model tailpipe and ventral nozzle have been made. The model was about one-third of full size, and the end was closed to simulate a blocked exhaust nozzle. Test data were obtained up to a ratio of tailpipe to ambient pressure of 4.0. The analytical work was done by using the PARC3D computational fluid dynamics program to predict the internal flow patterns and overall ventral system performance. The major results of these studies are as follows:

(1) A flow-turning total-pressure loss of about 5½ percent was measured in the model tested. This result is expected to be typical of full-size systems of similar geometry, but the loss should be lower for smaller ventral nozzles or

---

[iii] y+ = [(normal distance) (shear stress/density)$^{0.5}$]/kinematic viscosity.

13

systems with entrance flow-turning devices.

(2) Ventral nozzle flow and thrust coefficients were normal considering the measured flow-turning loss.

(3) A reverse (directed downstream) axial thrust component was measured, although the ventral nozzle axis was normal to the tailpipe centerline. This indicates that the flow turned more than the intended 90°.

(4) Paint streak flow visualization photographs and other data showed that a low-density region of separated vortical flow occurred at the upstream wall of the ventral duct. Flow was strong in the downstream part of the duct and tended to move toward the upstream wall from both the side and rear walls. This pattern persisted through the nozzle exit and caused the axial component measured by the thrust system.

(5) The modeling technique and the PARC3D computational code did a capable job of analyzing internal flow patterns and predicting system performance. Solutions were obtained for two computational grid densities. Both gave good results. The finer-grid solution produced more detailed flow patterns and predicted performance parameters, such as thrust and flow coefficient, within 1 percent of the measured values.

(6) Experience with the PARC3D code on this problem indicates that computational details could be improved further by using a two-equation turbulence model (such as the k-ϵ model) and preconditioning in flow regions of low (<0.1) Mach number.

References

1. Wynosky, T.A. and Szyszko, C.J., "V/STOL Deflector Aerodynamic Design Criteria - Geometric Variations Effects," AIAA Paper 73-1181, Nov. 1973.

2. Wynosky, T.A., Streib, R.A., and Usab, W.J., "V/STOL Deflector Concepts," AIAA Paper 74-1168, Oct. 1974.

3. Raman, G., Zaman, K.B.M.Q., and Rice, E.J., "Initial Turbulence Effect on Jet Evolution With and Without Tonal Excitation," AIAA Paper 87-2725, Oct. 1987. (Also, NASA TM-100178.)

4. Pulliam, T.H. and Steger, J.L., "Implicit Finite-Difference Simulations of Three Dimensional Compressible Flow," AIAA Journal, Vol. 18, No. 2, Feb. 1980, pp. 159-167.

5. Baldwin, B.S. and Lomax, H., "Thin-Layer Approximation and Algebraic Model for Separated Turbulent Flows," AIAA Paper 78-257, Jan. 1978.

6. Phares, W.J., Cooper, G.K., Jones, R.R., and Swafford, T.W., "Application of Computational Fluid Dynamics to Test Facility and Experiment Design," AIAA Paper 86-1733, June 1986.

7. Stokes, M.L. and Kneile, K.L., "A Search/Interpolation Algorithm for CFD Analysis," presented at the World Congress on Computational Mechanics, University of Texas, Austin, TX, Sept. 1986.

8. Soni, B.K., "Two- and Three-Dimensional Grid Generation for Internal Flow Applications of Computational Fluid Dynamics," 7th Computational Fluid Dynamics Conference, AIAA, 1985, pp. 351-359.

9. Wlatka, P.P. and Baning, P.J., "PLOT3D User's Manual," NASA TM-101067, 1990.

10. Harlow, F.H. and Nakayama, P.I., "Transport of Turbulence Energy Decay Rate," Los Alamos Scientific Laboratory Report LA-3854, Los Alamos, NM, 1968.

11. Kuethe, A.M. and Chow, C.Y., Foundations of Aerodynamics: Bases of Aerodynamic Design, 4th ed., John Wiley & Sons, Inc., New York, 1986.

12. Choi, Y.H., "Computation of Low Mach Number Compressible Flow," Ph.D. Thesis, The Pennsylvania State University, 1989.

13. Courant, R., Friedrichs, K.O., and Lewy, H., "Uber die Partiellen Differenzengleichungen der Mathematischen Physik," Mathematische Annalen, Vol. 100, 1928, pp. 32-74. (Translated to: "On the Partial Difference Equations of Mathematical Physics," IBM Journal of Research and Development, Vol. II, 1967, pp. 215-243.)

16. Abstract

Flow in a generic ventral nozzle system was studied experimentally and analytically with a block version of the PARC3D computational fluid dynamics program (a full Navier-Stokes equation solver) in order to evaluate the program's ability to predict system performance and internal flow patterns. For the experimental work a one-third-size model tailpipe with a single large rectangular ventral nozzle mounted normal to the tailpipe axis was tested with unheated air at steady-state pressure ratios up to 4.0. The end of the tailpipe was closed to simulate a blocked exhaust nozzle. Measurements showed about 5½-percent flow-turning loss, reasonable nozzle performance coefficients, and a significant aftward axial component of thrust due to flow turning more than 90°. Flow behavior into and through the ventral duct is discussed and illustrated with paint streak flow visualization photographs. For the analytical work the same ventral system configuration was modeled with two computational grids to evaluate the effect of grid density. Both grids gave good results. The finer-grid solution produced more-detailed flow patterns and predicted performance parameters, such as thrust and discharge coefficient, within 1 percent of the measured values. PARC3D flow visualization images are shown for comparison with the paint streak photographs. Modeling and computational issues encountered in the analytical work are discussed.